

SPATIO-TEMPORAL MONITORING OF URBAN HEAT ISLAND CHANGE USING SATELLITE IMAGES

Shahab Sherafati and M.R. Saradjian

Remote Sensing Division, Department of Surveying Engineering,
College of Engineering, University of Tehran, Tehran, Iran
Email: sh.sherafati@ut.ac.ir and sarajian@ut.ac.ir

KEY WORDS: Urban Climate, Urban Heat Island, Land Surface Temperature, Satellite Images

ABSTRACT

Urban Heat Island (UHI) phenomenon as a result of land cover change due to the urban expansion leads to the increase in temperature and affecting regional climate. In this study, multiple satellite images with different spatial and temporal resolutions have been used to determine Land Surface Temperature (LST) in Tehran metropolitan area. High temporal resolution of AVHRR images have been used as the main data source when investigating temperature variability in the urban area. However, in order to locate land cover types and relate them to AVHRR pixels, Thematic Mapper (TM) and Enhanced Thematic Mapper (ETM+) images have been exploited. In the preprocessing step, geometric and radiometric corrections have been made on the images. Then, appropriate cloud detection and masking has been applied to AVHRR images. The analysis shows that UHI appears more significant at afternoon and night hours. But the temperature of urban class is almost equal to its surrounding vegetation and bare soil classes at around noon. It has also been observed that there is no specific difference in UHI intense during the days throughout the year. However, it can be concluded that in the process of city expansion in years, UHI has been grown both spatially and in magnitude.

1 INTRODUCTION

Urban expansion leads to changes of thermal properties over urban area and makes it warmer than its surrounding non-urbanized areas, especially at night hours (Pu, et al., 2006). The main factors in creating UHI are: 1) changes in the physical characteristics of the surface like albedo and thermal capacity, 2) the decrease of surface moisture available for evapotranspiration and 3) changes in the radiative fluxes and near surface heat flow caused by geometric features of city surface (Dousset & Gourmelon, 2003). Extreme level of urban heat can be very harmful for human health. It can also increase the air pollution and amount of dangerous gases like carbon dioxide and ozone (Hu et al., 2010; Dousset et al., 2003).

The use of accurate data acquired by thermometer in ground stations has some spatial restrictions (especially because of relatively insufficient number of stations and their distribution). But remote sensing technology has made it possible to study LST with relatively high spatial resolution and show the relationship between UHI and land cover changes. Multiple types of thermal sensors with different spatial and temporal resolutions have been used for UHI monitoring. As these sensors have different number of thermal bands and physical characteristics, each one requires its own method of LST retrieval and atmospheric correction. The necessity of monitoring land cover changes in UHI researches and also differences in sensors resolution and capability makes it to use multiple sensors in urban temperature surveying. Pu et al. (2006) applied ASTER (Advanced Spaceborne Thermal Emission and Reflection Radiometer) and MODIS (MODerate resolution Imaging Spectroradiometer) images to measure LST in Yokohama city. They classified the region into six classes (water, forest, grass, wet agricultural, bare soil and built up) using three visible and NIR channels of ASTER and discussed the relation of NDVI and LST (Pu, et al., 2006). Hu and Jia, (2010) reviewed the relation of LST with NDVI and albedo using MODIS, ETM+, TM and MSS images (Hu & Jia, 2010). The objective of this study is to evaluate UHI spatial and temporal changes and find the relationship between land cover and LST using TM, ETM+ and AVHRR images. Figure 1 shows the flowchart of the procedure used.

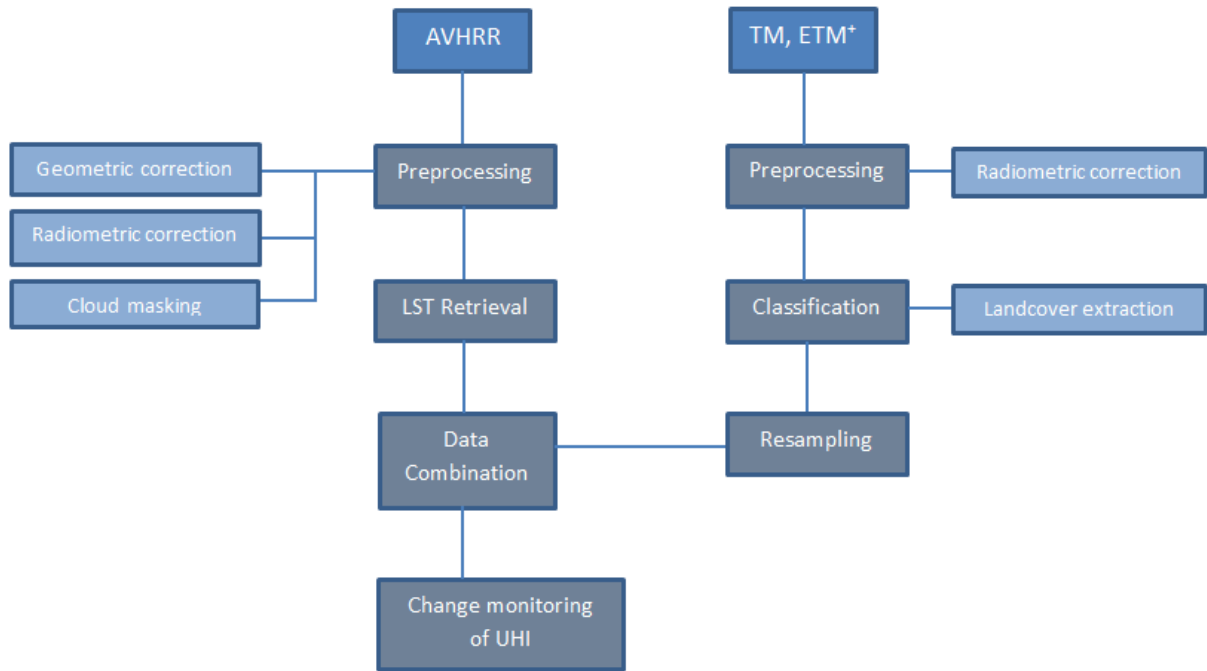


Figure 1: Flowchart of UHI changes monitoring using multi sensor images

2 STUDY AREA AND DATA SET

2.1 Study area

Tehran is located in the North of central part of Iran (52°E, 35°N) with a population over 8 million. It has semi dry and semi cold climate. The elevation difference in the northern and southern parts of the city is about 900 meter causing differences in the city temperature. The annual average temperature is about 17 degrees. In summer days it reaches up to 43° Celsius and in winter nights it is down to less than 0° (Mahmudian et al., 2006). Tehran has been capital of Iran since about 240 years ago (Mahmudian et al., 2006). Figure 2 shows Tehran expansion since 1856. The most significant urban growth occurred after 1925. Its area has also been increased about 300 square kilometers since 1974.

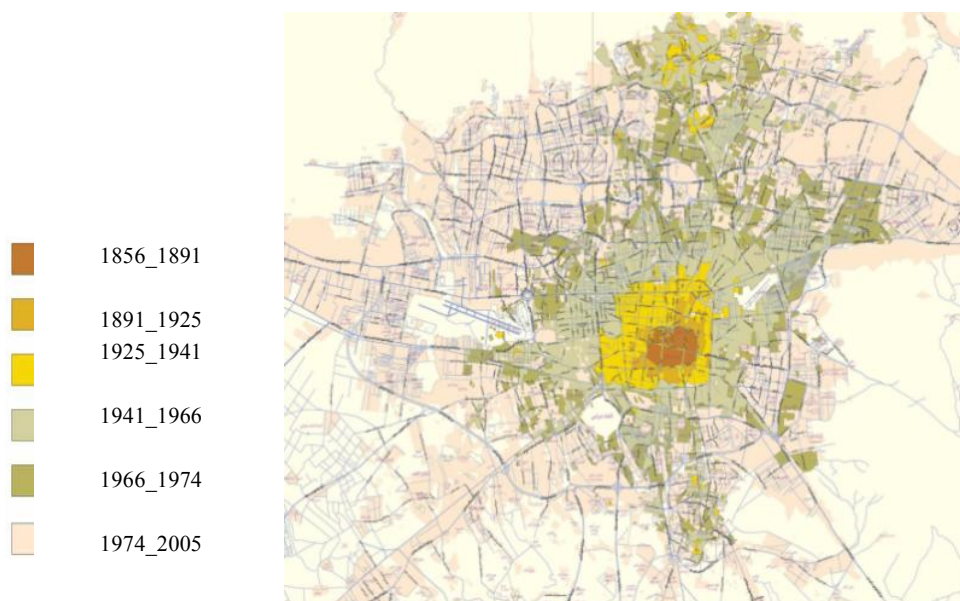


Figure 2: Tehran expansion steps since 1856.

2.2 Data sets and preprocessing

The AVHRR sensor has 5 spectral bands from visible to thermal infrared with spatial resolution of 1.1 km² in nadir. AVHRR instruments have been on board of NOAA platforms since 1978. NOAA has at least two satellites in orbit at all times, with one satellite crossing the equator in early morning and early evening and the other crossing the equator in the afternoon and late evening. This great temporal resolution makes it possible to study UHI changes even in the short periods of time like hours of a day.

Landsat TM and ETM+ images have also been used to find the relationship between LST and land cover types. The sensors with the spatial resolution of about 30 meters in their visible and near infrared bands are sufficient to discriminate land's major classes. TM and ETM+ images have been taken in 1985 and 2011, respectively.

In order to georeference the AVHRR images, sufficient number of ground control points (GCPs) were selected to calculate the coefficients for an affine transformation. Due to the low resolution of AVHRR images, most of the GCPs were selected from water bodies around the study area. The reason for adopting affine transformation is that the amount of discrepancy is different in north and east directions. As an example, Figure 3 shows the effect of transform on an image.

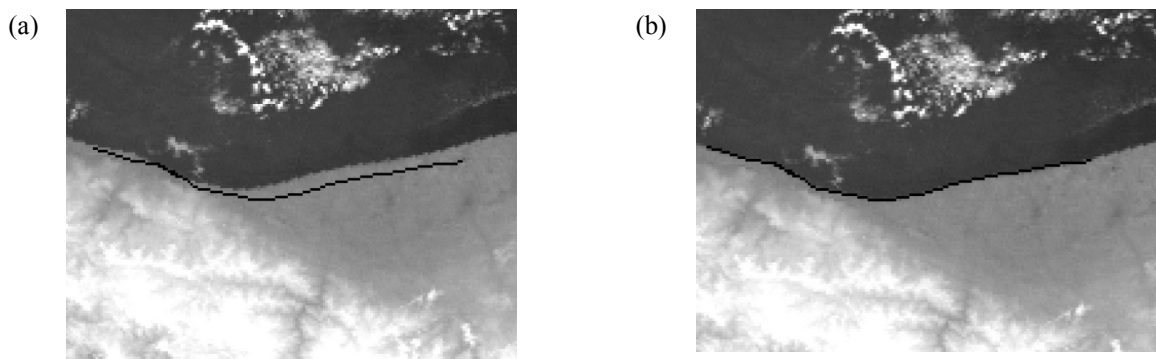


Figure 3: (a) Coastline in south of Caspian sea and north of Tehran before geometric correction, (b) Result of performing affine transformation to correct the image coordinate.

In this study, three cloud characteristics were used to find clear pixels. The first characteristic is cloud extreme reflection. If a pixel's albedo derived from channel 2 exceeds a threshold of 25%, it will be regarded as cloud pixel. This condition is only valid for the daytime images. Second condition is based on very low temperature of cloud. Any pixel with brightness temperature (calculated from channel 4) less than a specified threshold are not considered clear pixel. Depending on the season and hour of imaging, the threshold may vary. The final characteristic is cloud's very high variance. In a window of 9 pixels if the difference between maximum and minimum of temperatures was more than 3°, the center pixel may be considered as cloudy. If at least one of the above conditions is true, pixel will be flagged as cloud pixel.

3 METHODOLOGIES

3.1 LST retrieval

The top of atmospheric radiance measured by the AVHRR sensor is computed as a linear function of the input data (digital numbers that ranged from 0 to 1023 count) as follows (Anon., 2008):

$$E_i = S_i C + I_i$$

where E_i is the top of atmospheric radiance value in mW/(m²-sr-cm⁻¹), C is the input value, and S_i and I_i are respectively the scaled slope and intercept values for band i . During each scan line, in addition to earth targets, AVHRR views cold space behind it and its own blackbody target. Therefore using these two additional views, calibration coefficients (S_i and I_i) calculated for each band. Then conversion to brightness temperature from radiance is performed using the inverse of Planck's equation (Anon., 2008):

$$T = \frac{C_2 V}{\ln \left(\frac{C_1 V^2}{E} + 1 \right)}$$

Where T is the temperature (K) for radiance value (E), ν is the central wave number of each channel (cm^{-1}), $C_1 = 1.1910659 \times 10^{-5} \text{mW}/(\text{m}^2\text{-sr}\text{-cm}^{-1})$ and $C_2 = 1.438833 \times 10^{-5} \text{cm}\text{-K}$.

Sensors like AVHRR that have two thermal bands or more, make it possible to perform atmospheric correction by estimating differential absorption of their channels. This Split Window method is mainly used for sea surface temperature (SST), but in LST retrieval it has more conflicts (Kerr, et al., 2005). The main reason that causes less accuracy in estimating LST is the variability of land surface emissivity. Therefore, it is important to consider surface emissivity in split window equation. There are two main methods to derive surface emissivity from space. The first one is based on a relationship between emissivity and shortwave bands (0.5~1.1 μm). This method is almost empirical and the coefficients are surface dependent (Kerr, et al., 2005). The second method calculates emissivity by solving the radiometric equation at the surface in the thermal infrared. So this method needs more than one thermal band. An example of this method was proposed by Becker and Li (1990a). They used AVHRR channel 3 (3.7 μm) characteristic in day-night image pairs to measure emissivity. Because in channel 3 the daytime radiance is a combination of emitted radiance by the surface and reflected radiance due to Sun illumination, but the night-time radiance is just because of the emitted radiance. Therefore, the use of day-time and night-time images makes it possible to estimate the contribution of the reflected radiance and then emissivity (Kerr, et al., 2005).

Becker and Li (1990) proposed a method for LST retrieval for AVHRR as follows:

$$LST = \left[1.274 + \left[\frac{T_4 + T_5}{2} \left(1 + 0.15616 \frac{1 - \varepsilon}{\varepsilon} - 0.482 \frac{\Delta \varepsilon}{\varepsilon^2} \right) + \frac{T_4 - T_5}{2} \left(6.26 + 3.98 \frac{1 - \varepsilon}{\varepsilon} + 38.33 \frac{\Delta \varepsilon}{\varepsilon^2} \right) \right] \right]$$

$$\Delta \varepsilon = \varepsilon_4 - \varepsilon_5$$

$$\varepsilon = \frac{\varepsilon_4 + \varepsilon_5}{2}$$

Where T_4 and T_5 are respectively the brightness temperature in channels 4 and 5, and ε_4 and ε_5 represent emissivity in these two channels (Becker & Li, 1990).

4 IMPLEMENTATIONS AND ANALYSIS

In order to study UHI, land cover changes should be investigated first. Two Landsat satellite images have been used to show how land cover types have changed. The images have been classified to three classes (i.e. Urban, Bare soil and Vegetation) using maximum likelihood classification. Figures 4a and 4b show the classification maps of TM and ETM+ images, respectively. As it shows, the main direction of urban expansion is north-west although other areas also have some changes.

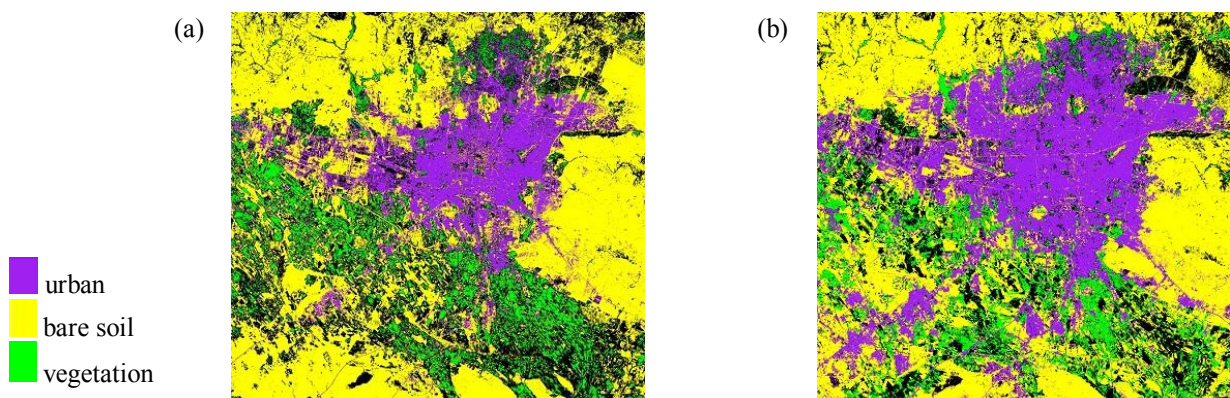


Figure 4: Classification of Tehran image using (a) Landsat TM in 1985, (b) Landsat ETM+ in 2011.

Figure 5 shows the diurnal changes of UHI, by temperature mean of each class measured in different hours of the day using AVHRR images. As it shows at night hours, the mean temperature in urban class is more than bare soil and vegetation classes (i.e. about 3 degrees), but around noon they are almost equal. The reason is that in the morning urban structures need more time to get warmer but in the afternoon when temperature decreases, it maintains heat more than vegetation and bare soil (Fabrizi, et al., 2010). It should be considered that Tehran has semi dry climate, but in cities surrounded by dense vegetation and forest, even around noon urban temperature is

higher than suburban areas. It can be concluded that for UHI expansion monitoring in a long period of time (several years), nighttime images are more appropriate than daytime images. This condition confines choosing proper sensor regarding to its capability in emissivity calculation, cloud detection and LST retrieval at night hours.

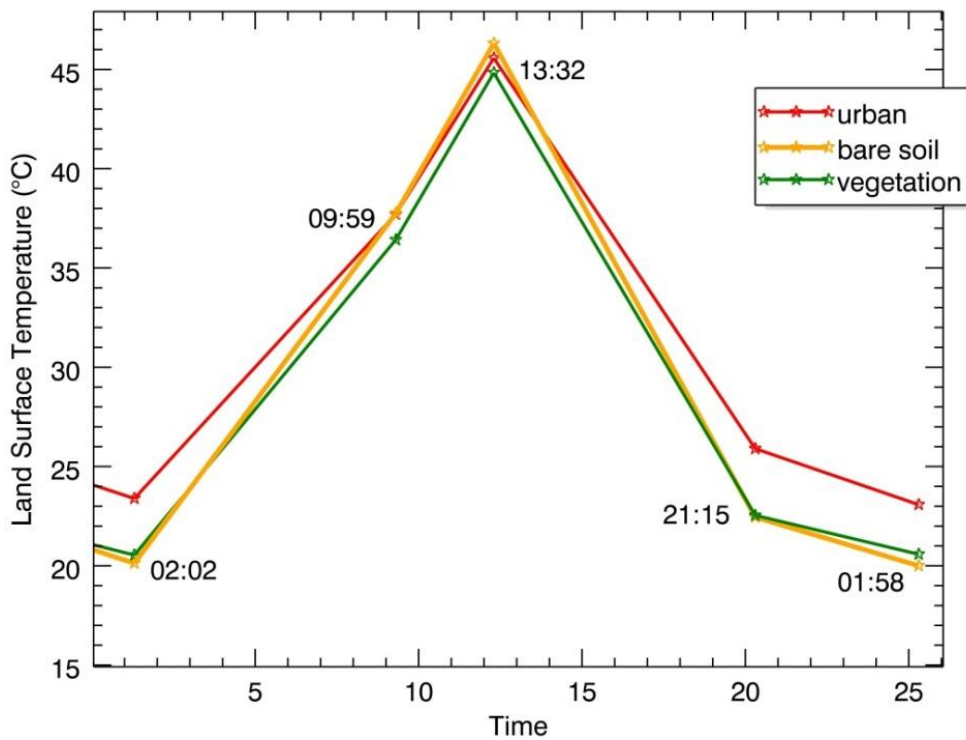


Figure 5: Diurnal cycle of LST in different classes measured by NOAA-AVHRR images in August 2010.

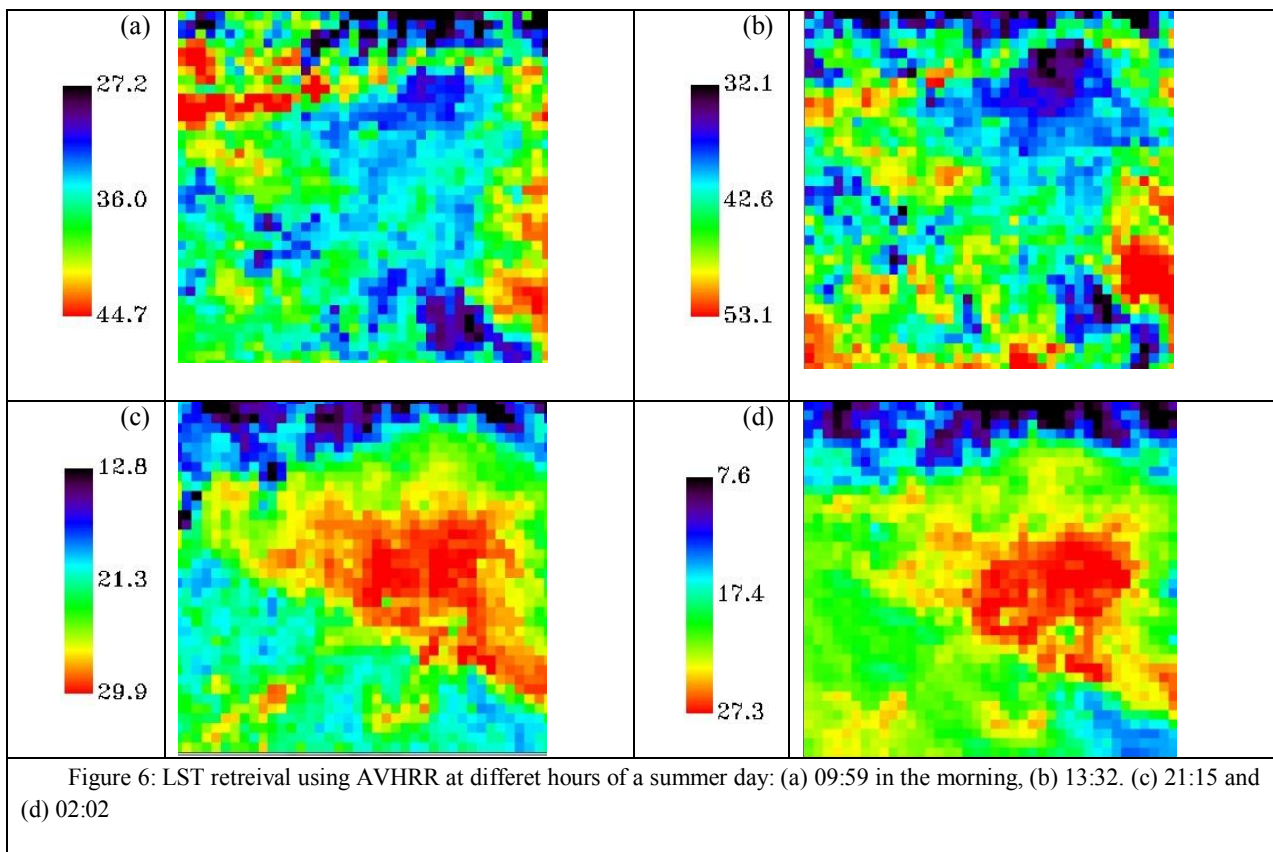


Figure 6: LST retrieval using AVHRR at different hours of a summer day: (a) 09:59 in the morning, (b) 13:32. (c) 21:15 and (d) 02:02

To find how UHI varies during days throughout the year, proper AVHRR nighttime images in 2010 in which Tehran was located near nadir and its pixels were not cloudy have been chosen to derive LST (Figure 7). As result

shows, in all nights of the year 2010, urban area is warmer than its surrounding vegetation and bare soil areas, and there is no significant difference in magnitude of UHI between summer and winter nights.

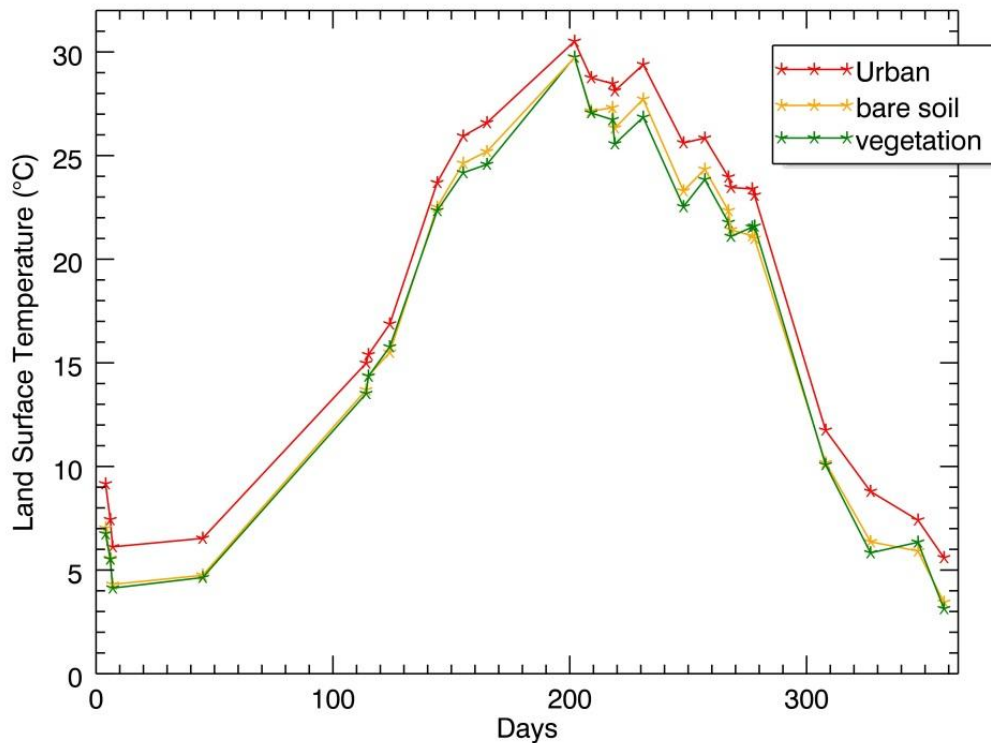


Figure 7: LST variation of the three classes during days throughout the year.

In order to get a further understanding of urban expansion impacts on LST increase, a NOAA9-AVHRR image taken in 1985 was combined with the TM classified image, and a NOAA19-AVHRR image taken in 2011 was combined with the ETM+ classified image. From the center point of the city outwards to suburb area, 10 buffer rings were generated with the interval of 3Km. In each buffer ring the percentages of urban pixels and mean temperature were calculated. Since two different NOAA sensors with different calibration were implemented, we used difference temperature (ΔT_p) instead of temperature itself as follows:

$$\Delta T_p = LST_p - LST_{base}$$

where LST_{base} is temperature mean of a selected area in southwest of Tehran in which landcover types have not changed during recent decades. The advantage of using ΔT_p instead of LST_p is that some sources of systematic errors like radiometric calibration errors and atmospheric effects are partially removed in the differencing procedure (Fabrizi, et al., 2010).

Figure 8 shows that in the center of the city where high percentage of urban class exists, ΔT_p is maximized, but temperature decreases as the distance from center of the city increases.

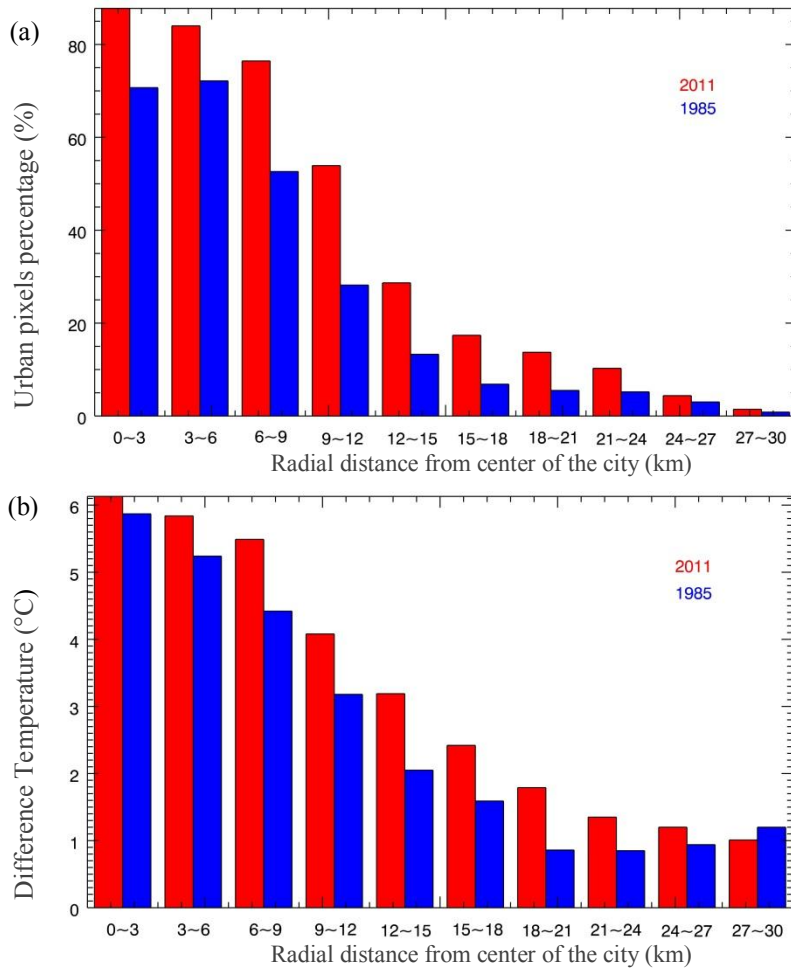


Figure 8: (a) Plot of urban percentage in different distance buffers in years 1985 and 2011. (b) ΔT Statistics in different distance buffers in years 1985 and 2011.

Figure 9 shows LST map deduced from the base area in 1985 and 2011.

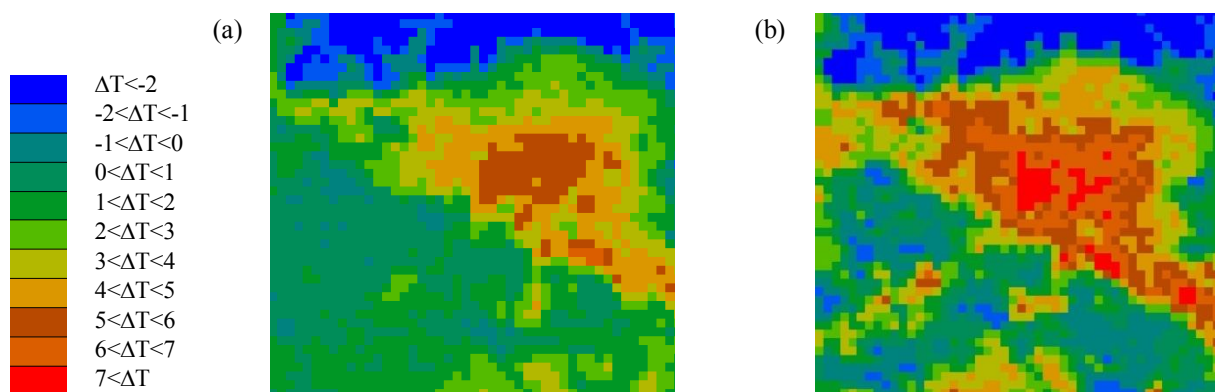


Figure 9: (a) LST map deduced from the base area in 1985, and (b) in 2011.

5 Conclusions

The capability of using satellite images in UHI monitoring has been illustrated in this study. When combining AVHRR thermal bands with Landsat visible and near infrared bands, remarkable relationship between land surface temperature and land cover types is observed. High temporal resolution AVHRR images represent that urban area in Tehran is warmer than its surrounding bare soil and vegetation areas especially at night hours. By generating

buffer distance rings from center of Tehran outwards to its suburb area, the role of urban expansion in increasing the LST from 1985 to 2011 is concluded.

References

- Anon., 2008. *NOAA Polar Orbiter Data User's Guide Section 3.3*. [Online] Available at: <http://www.ncdc.noaa.gov/oa/pod-guide/ncdc/docs/podug/html/c3/sec3-3.htm> [Accessed 12 Novembwr 2010].
- Anon., 2010. www.yale.edu/ceo/Documentation/DN_to_Kelvin.pdf. [Online] Available at: <http://www.yale.edu/ceo/>
- Becker, F. & Li, Z., 1990. Towards a local split window method over land surface. *international journal of remote sensing*, p. 369_393.
- Dousset, B. & Gourmelon, F., 2003. Satellite multi-sensor data analysis of urban surface temperatures and landcover. *ISPRS Journal of Photogrammetry & Remote Sensing*, pp. 43-54.
- Fabrizi, R., Bonafoni, S. & Biondi, R., 2010. Satellite and Ground-Based Sensor for the Urban Heat Island Analysis in the City of Rome. *Remote Sensing*, pp. 1400-1415.
- Hu, Y. & Jia, G., 2010. Influen of land use change on urban heat island derived from multi-sensor data. *International Journal of Climatology*, pp. 1382-1395.
- Kerr, Y. H., Lagouarde, J. P., Nerry, F. & Otle, C., 2005. Land surface temperature retrieval techniques and applications. In: *Thermal Remmote Sensing in Land Surface Processes*. s.l.:s.n., pp. 33-109.
- Mahmudian, A. a., Ghasemi, H., Houshmand fini, g. r. & Artidar, R., 2006. *A glance at Tehran from the beginnig uptill now.* Tehran: GITASHENASI Geographical & Cartographic Institute.
- Nakano, M. & Kalpoma, K. A., 2004. *Automatic GCP creation for NOAA AVHRR image Geometric Correction*. Anchorage, AK, IEEE international, pp. 3733-3735.
- Poli, G., Adembri, G., Gherardelli, M. & Tommasini, M., 2010. *Dynamic threshold cloud detection algorithm improvement for AVHRR seviri images*. s.l., IEEE, p. 4146_4149.
- Pu, R., Gong, P., Michishita, R. & Sasagawa, T., 2006. Assessment of multi-resolution and multi-sensor data for urban surface temperature retrieval. *Remote Sensing of Environment*, pp. 211-225.
- Sobrino, J. A., Jimenez-Munoz, J. C. & Polini, L., 2004. Land surface temperature retrieval from LANDSAT TM5. *Remote Sensing of Environment*, pp. 434-440.
- Streutker, D., 2003. Satellite-measured growth of the urban heat island of Houston, Texas. *Remote Sensing of Environment*, pp. 282-289.
- Valor, E. & Caselles, V., 1996. Mapping land surface emissivity from NDVI: application to European, and south American Areas. *Remotr Sensing of Environment*, p. 167_184.
- Weng, Q., Lu, D. & Schubring, J., 2004. Estimation of land surface temperature-vegetation abundance relationship for urban heat island studies. *Remote Sensing of Environment*, p. 467_483.
- Xu, Y. & Qin, Z. L. J., 2008. *Comparative analysis of urban heat island and associated land cover change based in suzhou city using landsat data*. s.l., IEEE, pp. 316-319.
- Zhu, S.-Y., Yin, Q. & Kuang, D.-B., 2006. Using characteristic spectral bands of OMIS1 imaging spectrometer to retrieve urban land surface temperature. *International Journal of Remote Sensing*, pp. 1661-1676.